Fluence and polarisation dependence of GaAs based Lateral Photo-Dember terahertz emitters

D. McBryde,[1],* M. E. Barnes,[1] S. A. Berry,[1] P. Gow,[1] H. E. Beere,[2] D. A. Ritchie,[2] and V. Apostolopoulos[1]

[1]*Physics and Astronomy, University of Southampton, Southampton SO17 1BJ, UK*
[2]*Semiconductor Physics, Cavendish Laboratory, University of Cambridge, CB3 0HE, UK*
*duncan.mcbryde@southampton.ac.uk

Abstract: We characterise THz output of lateral photo-Dember (LPD) emitters based on semi-insulating (SI), unannealed and annealed low temperature grown (LTG) GaAs. Saturation of THz pulse power with optical fluence is observed, with unannealed LTG GaAs showing highest saturation fluence at 1.1 ± 0.1 mJ cm^{-2}. SI-GaAs LPD emitters show a flip in signal polarity with optical fluence that is attributed to THz emission from the metal-semiconductor contact. Variation in optical polarisation affects THz pulse power that is attributed to a local optical excitation near the metal contact.

OCIS codes: (320.7130) Ultrafast processes in condensed matter, including semiconductors; (300.6495) Spectroscopy, terahertz.

References and links

1. T. Dekorsy, H. Auer, H. J. Bakker, H. G. Roskos, and H. Kurz, "THz electromagnetic emission by coherent infrared-active phonons." Phys. Rev. B **53**, 4005–4014 (1996).
2. M. C. Beard, G. M. Turner, and C. A. Schmuttenmaer, "Subpicosecond carrier dynamics in low-temperature grown GaAs as measured by time-resolved terahertz spectroscopy," J. Appl. Phys. **90**, 5915 (2001).
3. K. Liu, J. Z. Xu, T. Yuan, and X.-C. Zhang, "Terahertz radiation from InAs induced by carrier diffusion and drift," Phys. Rev. B **73**, 155330 (2006).
4. P. Gu, M. Tani, S. Kono, K. Sakai, and X.-C. Zhang, "Study of terahertz radiation from InAs and InSb," J. Appl. Phys. **91**, 5533 (2002).
5. N. Sarukura, H. Ohtake, S. Izumida, and Z. Liu, "High average-power THz radiation from femtosecond laser-irradiated InAs in a magnetic field and its elliptical polarization characteristics," J. Appl. Phys. **84**, 654 (1998).
6. M. B. Johnston, D. Whittaker, A. Corchia, A. G. Davies, and E. Linfield, "Simulation of terahertz generation at semiconductor surfaces," Phys. Rev. B **65**, 165301 (2002).
7. M. B. Johnston, D. M. Whittaker, A. Corchia, A. G. Davies, and E. H. Linfield, "Theory of magnetic-field enhancement of surface-field terahertz emission," J. Appl. Phys. **91**, 2104 (2002).
8. R. Kersting, K. Unterrainer, G. Strasser, H. Kauffmann, and E. Gornik, "Few-Cycle THz Emission from Cold Plasma Oscillations," Phys. Rev. Lett. **79**, 3038–3041 (1997).
9. M. E. Barnes, D. McBryde, G. J. Daniell, G. Whitworth, A. L. Chung, A. H. Quarterman, K. G. Wilcox, A. Brewer, H. E. Beere, D. A. Ritchie, and V. Apostolopoulos, "Terahertz emission by diffusion of carriers and metal-mask dipole inhibition of radiation." Opt. Express **20**, 8898–906 (2012).
10. G. Klatt, F. Hilser, W. Qiao, M. Beck, R. Gebs, A. Bartels, K. Huska, U. Lemmer, G. Bastian, M. B. Johnston, M. Fischer, J. Faist, and T. Dekorsy, "Terahertz emission from lateral photo-Dember currents." Opt. Express **18**, 4939–4947 (2010).
11. G. Klatt, B. Surrer, D. Stephan, O. Schubert, M. Fischer, J. Faist, A. Leitenstorfer, R. Huber, and T. Dekorsy, "Photo-Dember terahertz emitter excited with an Er:fiber laser," Appl. Phys. Lett. **98**, 021114 (2011).
12. G. Klatt, F. Hilser, W. Chao, R. Gebs, A. Bartels, K. Huska, U. Lemmer, G. Bastian, M. B. Johnston, M. Fischer, J. Faist, and T. Dekorsy, "Intense terahertz generation based on the photo-Dember effect," OSA / CLEO / QELS 2010 (2010).

#200985 - $15.00 USD Received 8 Nov 2013; revised 13 Dec 2013; accepted 27 Jan 2014; published 4 Feb 2014

13. W. Qiao, D. Stephan, M. Hasselbeck, Q. Liang, and T. Dekorsy, "Low-temperature THz time domain waveguide spectrometer with butt-coupled emitter and detector crystal," Opt. Express **20**, 19769 (2012).
14. M. E. Barnes, S. A. Berry, P. Gow, D. McBryde, G. J. Daniell, H. E. Beere, D. A. Ritchie, and V. Apostolopoulos, "Investigation of the role of the lateral photo-Dember effect in the generation of terahertz radiation using a metallic mask on a semiconductor," Opt. Express **21**, 16263 (2013).
15. K. Drexhage, "Influence of a dielectric interface on fluorescence decay time," J. Lumin. **1-2**, 693–701 (1970).
16. S. Park, M. Melloch, and A. Weiner, "Analysis of terahertz waveforms measured by photoconductive and electrooptic sampling," IEEE J. Quantum Electron. **35**, 810–819 (1999).
17. T. S. Sosnowski, T. B. Norris, H. H. Wang, P. Grenier, J. F. Whitaker, and C. Y. Sung, "High-carrier-density electron dynamics in low-temperature-grown GaAs," Appl. Phys. Lett. **70**, 3245 (1997).
18. S. Rihani, R. Faulks, H. E. Beere, H. Page, I. S. Gregory, M. Evans, D. A. Ritchie, and M. Pepper, "Effect of defect saturation on terahertz emission and detection properties of low temperature GaAs photoconductive switches," Appl. Phys. Lett. **95**, 051106 (2009).
19. G. Segschneider, F. Jacob, T. Löffler, H. Roskos, S. Tautz, P. Kiesel, and G. Döhler, "Free-carrier dynamics in low-temperature-grown GaAs at high excitation densities investigated by time-domain terahertz spectroscopy," Phys. Rev. B **65**, 125205 (2002).
20. Y. Shi, Y. Yang, X. Xu, S. Ma, W. Yan, and L. Wang, "Ultrafast carrier dynamics in Au/GaAs interfaces studied by terahertz emission spectroscopy," Appl. Phys. Lett. **88**, 161109 (2006).
21. P. G. Huggard, C. J. Shaw, J. A. Cluff, and S. R. Andrews, "Polarization-dependent efficiency of photoconducting THz transmitters and receivers," Appl. Phys. Lett. **72**, 2069 (1998).
22. M. Tani, M. Herrmann, and K. Sakai, "Generation and detection of terahertz pulsed radiation with photoconductive antennas and its application to imaging," Meas. Sci. Technol. **13**, 1739–1745 (2002).
23. M. Tani, S. Matsuura, K. Sakai, and S. Nakashima, "Emission characteristics of photoconductive antennas based on low-temperature-grown GaAs and semi-insulating GaAs." Appl. Opt. **36**, 7853–7859 (1997).
24. I. S. Gregory, "The development of a continuous-wave terahertz imaging system," Ph.D. thesis, (2004).
25. J. K. Luo, H. Thomas, D. V. Morgan, and D. Westwood, "Transport properties of GaAs layers grown by molecular beam epitaxy at low temperature and the effects of annealing," J. Appl. Phys. **79**, 3622 (1996).
26. E. S. Harmon, M. R. Melloch, J. M. Woodall, D. D. Nolte, N. Otsuka, and C. L. Chang, "Carrier lifetime versus anneal in low temperature growth GaAs," Appl. Phys. Lett. **63**, 2248 (1993).
27. P. Grenier and J. F. Whitaker, "Subband gap carrier dynamics in low-temperature-grown GaAs," Appl. Phys. Lett. **70**, 1998 (1997).
28. D. Look, D. Walters, and M. Manasreh, "Anomalous Hall-effect results in low-temperature molecular-beam-epitaxial GaAs: Hopping in a dense EL2-like band," Phys. Rev. B **42**, 2–5 (1990).
29. S. Fleischer, C. D. Beling, S. Fung, W. R. Nieveen, J. E. Squire, J. Q. Zheng, and M. Missous, "Structural and defect characterization of GaAs and AlGaAs grown at low temperature by molecular beam epitaxy," J. Appl. Phys. **81**, 190 (1997).
30. I. S. Gregory, C. Baker, W. R. Tribe, M. Evans, H. E. Beere, E. H. Linfield, A. G. Davies, and M. Missous, "High resistivity annealed low-temperature GaAs with 100 fs lifetimes," Appl. Phys. Lett. **83**, 4199 (2003).
31. S. Gupta, M. Y. Frankel, J. A. Valdmanis, J. F. Whitaker, G. A. Mourou, F. W. Smith, and A. R. Calawa, "Subpicosecond carrier lifetime in GaAs grown by molecular beam epitaxy at low temperatures," Appl. Phys. Lett. **59**, 3276 (1991).
32. Y. Jin, X. F. Ma, G. A. Wagoner, M. Alexander, and X.-C. Zhang, "Anomalous optically generated THz beams from metal/GaAs interfaces," Appl. Phys. Lett. **65**, 682 (1994).
33. W. G. Heitman and P. van den Berg, "Diffraction of Electromagnetic Waves by a Semi-Infinite Screen in a Layered Medium," Can. J. Phys. **53**, 1305–1317 (1975).
34. S. E. Ralph and D. Grischkowsky, "Trap-enhanced electric fields in semi-insulators: The role of electrical and optical carrier injection," Appl. Phys. Lett. **59**, 1972 (1991).
35. D. S. Kim and D. S. Citrin, "Efficient terahertz generation using trap-enhanced fields in semi-insulating photoconductors by spatially broadened excitation," J. Appl. Phys. **101**, 053105 (2007).

1. Introduction

Terahertz emission from the photo-Dember (PD) effect arises from the differing mobilities of holes and electrons within a semiconductor [1]. An ultra-fast laser pulse generates carriers at the surface of a semiconductor. The surface imposes a boundary condition on the diffusion current as carriers cannot go beyond the semiconductor-air surface. The boundary condition constrains carriers to diffuse into the bulk semiconductor. Different diffusivities of holes and electrons create a net dipole oriented parallel to the surface normal of the material. Carrier diffusion occurs within a picosecond time scale with the rate of change of the diffusion current governing the terahertz emission [2–4]. THz emission using the photo-Dember effect can be

#200985 - $15.00 USD Received 8 Nov 2013; revised 13 Dec 2013; accepted 27 Jan 2014; published 4 Feb 2014

optimised by orienting the semiconductor surface at 45° or using strong magnetic fields to change the dipole orientation [5–7]. The photo-Dember effect is distinct from the surface field effect [8] where a drift current is caused by pinning the Fermi energy to the surface of the semiconductor.

The surface boundary imposed on the diffusion current creates the dipole in the normal photo-Dember effect. In the lateral photo-Dember (LPD) effect a radiative terahertz dipole is created by partially masking the semiconductor surface with a metal layer. By focussing an ultrafast laser, with above band-gap energy, on the metal-semiconductor boundary a spatially asymmetrical distribution of carriers forms near the metal-semiconductor interface [9,10]. Such a device gives intense THz emission as observed by [10–14]. The terahertz emission has been attributed to an asymmetrical diffusion current due to the initial asymmetrical carrier distribution. However, we have investigated this argument and demonstrated that an asymmetrical carrier distribution results in no net lateral diffusion current [9,14]. An asymmetric carrier distribution results in quadrupole emission with no emission detected in the direction of the detector. We have explained the detected terahertz emission by taking into account dipole quenching that occurs near the metal mask [9, 14]. Dipoles formed under the metal are quenched due to destructive interference from the reflection from the metal mask [15]. Dipoles formed elsewhere are free to radiate and it is these radiative dipoles that are responsible for the detected terahertz emission. We have supported this argument with finite element modelling and found the results in agreement with the signal polarity of our measurements [9, 14], which is opposite to the polarity predicted in [10]. The resulting THz pulses in the LPD effect have higher bandwidth compared with photoconductive antenna structures, but approximately an order of magnitude less output power [10].

Terahertz emission from the LPD effect is expected to be affected by the difference in mobilities of the carriers and carrier lifetime. Carrier mobility defines the strength of the created dipole; carrier lifetime affects the saturation fluence and the decay of the photocurrent [16]. We present measurements of the THz emission of LPD emitters based on semi-insulating (SI) GaAs, unannealed low temperature grown (LTG) GaAs and annealed LTG GaAs. We obtain saturation data which demonstrate the greatest THz emission signal for unannealed LTG GaAs due to a high saturation fluence. The annealed LTG GaAs based LPD emitter shows greater efficiency in THz generation at low fluences and exhibits a lower saturation fluence that is attributed to the longer carrier lifetime. The annealed LTG GaAs emitter also shows a changing shape of the time domain scan and a variation of THz pulse power with fluence that indicates a change in carrier dynamics with fluence. We attribute this to saturation of the defect states which has been shown to increase carrier lifetimes in annealed LTG GaAs [17–19]. SI-GaAs demonstrates the lowest saturation fluence and a flip in signal polarity in the time domain electric field as the optical fluence increases. We attribute the flip in signal polarity to band bending of the Schottky barrier between the gold and the semiconductor [20]. We confirm this by fabricating an identical emitter with an insulating layer demonstrating no flip in signal polarity. Optical polarisation affects LPD emitter performance, with peak THz emission occurring at perpendicular polarisation relative to the semiconductor-metal boundary. This polarisation dependency has similar behaviour to that observed in photoconductive antennas [21]. We explain the polarisation dependency with a finite element simulation of the electric field of the optical pulse for different polarisations under the LPD metal mask.

2. Fitting model

To determine the fluence at which saturation occurs a one dimensional model based on the LPD emitter geometry was created. Taking the geometry of the emitter into account results in a better fit compared with the model used in [14, 22, 23]. In the LPD effect the total diffusion current

#200985 - $15.00 USD Received 8 Nov 2013; revised 13 Dec 2013; accepted 27 Jan 2014; published 4 Feb 2014

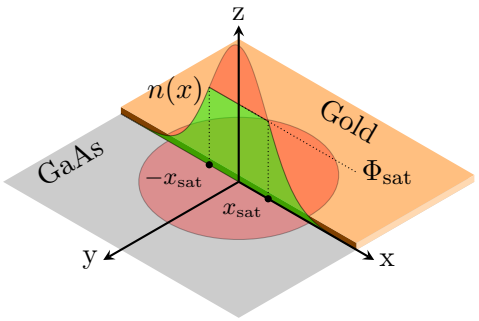

Fig. 1. A diagram showing the geometry of the fitting model in relation to the LPD emitter. A laser pulse, shown in red, illuminates the edge of the LPD emitter causing carriers to be generated along the boundary as a function of fluence, with the carrier density defined as $n(p,c,\Phi_{\text{sat}},x)$, shown in green. The carrier density saturates at an optical fluence of Φ_{sat}. The co-ordinate scheme shown is common to Figs. 3, 4 and 5

that will contribute to the THz emission is proportional to the difference of carrier concentration on the metal edge, where it is highest, to the edge of the optical spot furthest away from the metal edge, where it is zero. Thus we assume that the diffusion current is proportional to the carrier concentration N only along the metal boundary, shown as the green region in Fig. 1. We assume that the terahertz emission is proportional to the rate of change of current which is proportional to the maximum carrier concentration on the boundary. In our model we assume that the number of carriers generated is proportional to the fluence, Φ, of the beam up to a maximum value of Φ_{sat} shown in Fig. 1. The fluence Φ of the pump beam with average power p and radius c can be spatially described as a Gaussian function, and so the fluence along the border for a centred beam spot is

$$\Phi(x) = \frac{p}{2\pi c^2}\exp\left(-\frac{x^2}{2c^2}\right). \tag{1}$$

This function is shown in Fig. 1 in red. It is assumed that the carrier density n is proportional to the fluence which is saturated at Φ_{sat}. This creates a Gaussian distribution of carrier density that is restricted at Φ_{sat} within the range of x_{sat} and $-x_{\text{sat}}$, shown in Fig. 1, which is

$$n(p,c,\Phi_{\text{sat}},x) \propto \begin{cases} \frac{p}{2\pi c^2}\exp\left(-\frac{x_{\text{sat}}^2}{2c^2}\right), & \text{for } |x| < x_{\text{sat}}; \\ \frac{p}{2\pi c^2}\exp\left(-\frac{x^2}{2c^2}\right), & \text{for } |x| > x_{\text{sat}}. \end{cases} \tag{2}$$

The integration of this function represents the sum of carriers along the boundary, N, and is shown in the green region in figure Fig. 1. The integration of expression 2 can be shown to be

$$\begin{aligned} \int_{-\infty}^{\infty} n(p,c,\Phi_{\text{sat}},x)\mathrm{d}x = 2\sqrt{2}c\Phi_{\text{sat}}\mathbb{R}\left\{\left[\ln\left(\frac{p}{2\pi c^2\Phi_{\text{sat}}}\right)\right]^{1/2}\right\} \\ + \frac{1}{\sqrt{2\pi}}\frac{p}{c}\,\text{erfc}\left(\mathbb{R}\left\{\left[\ln\left(\frac{p}{2\pi c^2\Phi_{\text{sat}}}\right)\right]^{1/2}\right\}\right). \end{aligned} \tag{3}$$

where $\mathbb{R}$ is the real part of the function. Since we assume E_{THz} is proportional to N, equation 3 is the term fitted to our results to determine Φ_{sat}, where E_{THz} is the spectral power. Power and

#200985 - $15.00 USD Received 8 Nov 2013; revised 13 Dec 2013; accepted 27 Jan 2014; published 4 Feb 2014

spot size are determined by the experiment, therefore the only parameter to fit is the saturation fluence.

3. Experimental details

To observe the effect of varying pump fluence on output THz emission a typical THz-TDS apparatus was used with a range of LPD emitters patterned on unannealed LTG GaAs, annealed LTG GaAs and SI-GaAs. A 80 MHz repetition rate Ti:Sapphire laser at 800 nm wavelength, pulse duration $<$100 fs, was used as the beam source with a commercial LTG GaAs (Menlo Tera T8) antenna used as a receiver. All LPD emitters were grown on (100) cut SI-GaAs substrate. The LTG GaAs LPD emitters consist of a 1 μm layer of LTG GaAs grown at 230°C on a 100 nm AlAs layer on a SI-GaAs substrate. One of the two emitters was annealed, post-growth, at 600°C. Each sample was partially masked by gold to form a boundary between the gold and semiconductor, such an interface forms a LPD emitter. Varying the pump beam power and beam radius (defined as $1/e^2$ of the peak intensity) allows the optical fluence to be changed. The laser beam was found to be spatially Gaussian in shape, we created different spot sizes by moving the 12.7 mm focal length achromatic doublet focusing lens. We determined the divergence of the beam with knife-edge measurements to determine the width of the Gaussian beam at different lens positions. The power of the terahertz pulse was determined by calculating the spectral power of the pulse, defined as the sum of the real part of the Fourier transform of the time-domain terahertz pulse.

4. Results

4.1. Fluence dependency

The results of unannealed LTG GaAs, output THz power as a function of optical fluence are shown in Fig. 2(a). The LPD emitter based on unannealed LTG GaAs demonstrates a linear relationship between output THz power. Fitting equation 3 to the data gives an average value of $\Phi_{\text{sat}} = 1.1 \pm 0.1$ mJ cm^{-2}. This fluence is above the damage threshold for GaAs, demonstrating a lack of observable saturation within the measured data. Of the set of materials tested, unannealed LTG GaAs demonstrates the highest output power with optical fluence. However, it is the least efficient at low optical fluences compared to SI and annealed GaAs. We believe that this observed saturation is due to thermal damage from the optical beam as damage was observed on the gold mask. As the number of trap states in unannealed LTG GaAs are of the order of 5×10^{19} cm^{-2} they are greater than the number of carriers generated [24]. Most carriers are captured from the trap states and this reservoir of carriers is not depleted. Therefore, the reason that unannealed LTG GaAs exhibits higher saturation fluence in relation to the other materials is its short carrier lifetime due to the trap states, of approximately 100 fs which is comparable to the optical pulse temporal width.

Annealed LTG GaAs is frequently used as a photoconductive terahertz emitter due to sub-picosecond carrier lifetime and higher dark resistivity as these are ideal qualities in a photoconductive switch. Unannealed LTG GaAs suffers from low dark resistivity due to conduction from excess arsenic and charge saturation and conduction from the EL2 band [25–28]. Annealing the samples at high temperatures (600°C) creates precipitates from the excess arsenic [29]. Annealing increases the resistivity but increases the carrier lifetime [26]. The resistivity of LTG GaAs increases by five orders of magnitude when annealed at 600°C but carrier lifetime is increased from 90 fs to 1.6 ps [30].

The results of annealed LTG GaAs, output THz power as a function of optical fluence are shown in Fig. 2(b). The annealed LTG GaAs LPD emitter demonstrates two distinct regions of fluence dependence as shown in Fig. 2(b). This behavior is not compatible with our model

#200985 - $15.00 USD Received 8 Nov 2013; revised 13 Dec 2013; accepted 27 Jan 2014; published 4 Feb 2014

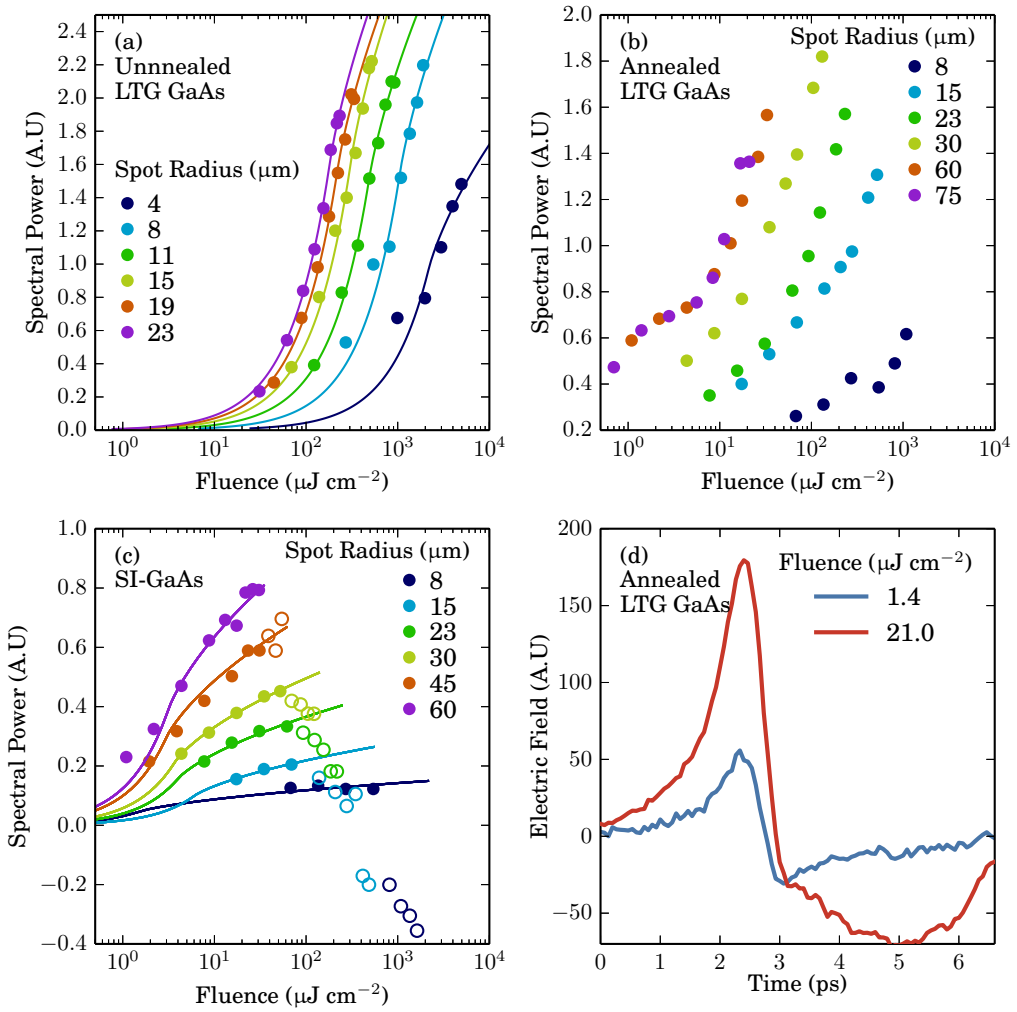

Fig. 2. (a), (b) and (c) show the spectral power of the THz pulse with optical fluence grouped by optical spot size for unannealed and annealed LTG GaAs and SI-GaAs. Circled data excluded from the fit. Curves from equation 3 are fitted to (a) and (c) to determine Φ_{sat}. (d) shows the terahertz time domain scan for the annealed GaAs LPD emitter at 1 μJ cm^{-2} and 21 μJ cm^{-2}, with spot radius 75 μm and optical powers 10 mW and 300 mW. The same power units are used in all graphs.

description and so equation 3 does not fit Fig. 2(b). For fluences less than 3 μJ cm^{-2}, the emitter shows signs of saturation with decreasing gradient for spot radii 60 μm and 75 μm. Within this fluence region the output THz power is greater than that of unannealed LTG GaAs and SI-GaAs, demonstrating that the annealed LTG GaAs emitter shows greater efficiency at low fluences. In Fig. 2(b) the gradient of the THz power increases past this fluence region. The time domain signal changes between the two regions as shown in Fig. 2(d). At 1 μJ cm^{-2} the electric field of the time domain terahertz pulse increases linearly from 3 to 6 ps, whereas above 10 μJ cm^{-2} the electric field decreases and rises between 3 and 6 ps, as shown in Fig. 2(d). Annealing the sample reduces the total number of trap states to 10^{18} cm^{-2} [31], comparable to the number of excited free carriers. The change in carrier dynamics within annealed LTG GaAs with fluence

#200985 - $15.00 USD Received 8 Nov 2013; revised 13 Dec 2013; accepted 27 Jan 2014; published 4 Feb 2014

has been observed with THz-TDS due to trap saturation [17]; this variation of carrier lifetime with fluence is compatible with the change of the time domain signal seen in our measurements. At low optical fluences, where the number of trap states is greater than the number of excited carriers, carrier lifetime is determined by the capture rate from the conduction band to trap states. As optical fluence increases, the trap states become fully occupied with carriers and the trap rate is decreased and becomes dependent on the recombination time from the trap state to the valence band. Increasing the optical fluence increases the recombination time of the carriers which affects the time domain past 3 ps, as shown in Fig. 2(d). In the rate equations described in Sosnowski et al. [17] when saturation is reached more optical light is used to generate free carriers. Since we expect the THz signal to be proportional to the number of free carriers, this also explains the abrupt change in pulse power shown in Fig. 2(b) at fluence 10 μJ cm^{-2}. The thickness of the grown material for both LTG GaAs samples allows for a non-negligible amount of optical power to reach the SI-GaAs substrate, however the THz emission from SI-GaAs is small compared with both LTG GaAs samples and does not affect the results significantly.

The results of SI-GaAs, output THz power as a function of optical fluence are shown in Fig. 2(c). The SI-GaAs LPD emitter produces less powerful terahertz emission than either annealed or unannealed LTG GaAs. It is expected that SI-GaAs has a lower saturation fluence due to longer carrier lifetime. The output power is less than half that of unannealed LTG GaAs as shown in Fig. 2(a). SI-GaAs based LPD emitters exhibit a point of inflection at 15.5 $\pm$ 3 μJ cm^{-2} as shown in Fig. 2(c). Beyond this fluence the output power of the emitter decreases and the polarity of the pulse inverts. The flip in signal polarity depends strongly on the optical beam position relative to the semiconductor-metal interface. Figure 3(a) and (b) shows that this effect is only observable within $\pm$20 μm of the semiconductor-metal boundary, whereas LPD emission occurs over 100 μm. The set of time-domain scans in Figs. 3(a) and (b) use an optical spot radius of 15 μm and 290 mW optical power, yielding a fluence of 506 μJ cm^{-2}. Figure 3(a) shows the time domain for -20, 0 and 20 μm optical spot positions relative to the metal-semiconductor. Figure 3(b) combines sets of time-domain scans with lateral position relative to the gold mask, showing a signal inversion on the gold boundary, positioned at 0 μm.

The decrease and inversion of the polarity is attributed to a competing THz emission mechanism that dominates the LPD effect in SI-GaAs samples at fluences greater than 300 μJ cm^{-2}. This competing effect causes fluence dependence above Φ_{sat}, as shown in 2(c), to decrease rapidly. Thus the value determined for Φ_{sat} is determined not only by the intrinsic carrier saturation but also by the relative strength of the competing generation mechanism. Fluence dependent terahertz polarity inversion from gold-GaAs interfaces has been previously observed [32]. By fabricating an emitter with an insulating polyimide layer between the metal and semiconductor we were able to demonstrate THz emission from SI-GaAs and unannealed LTG GaAs without loss of performance; the results for the LTG GaAs are shown in Fig. 3(c). This shows that the LPD emission mechanism is dominated by carrier diffusion instead of THz emission from a Schottky barrier. No flip in the signal polarity was observed for the SI-GaAs sample with the insulating layer for fluences above 100 μJ cm^{-2}, showing that the competing terahertz generation mechanism is emission due to the metal-semiconductor interface. The change in polarity can be explained due to the reversal of the electric field within the depletion layer at the metal-semiconductor contact [20]. At low fluences electrons diffuse from the metal interface to the semiconductor, but at high carrier concentrations the current reverses due to band bending caused by the increased carrier density and the lower Fermi energy in the metal [20]. Figure 3(b) shows the polarity inversion occurring within a region smaller than the spot radius. We attribute this behaviour to the spatial resolution of the time domain scans determined by the width of the depletion region.

#200985 - $15.00 USD Received 8 Nov 2013; revised 13 Dec 2013; accepted 27 Jan 2014; published 4 Feb 2014

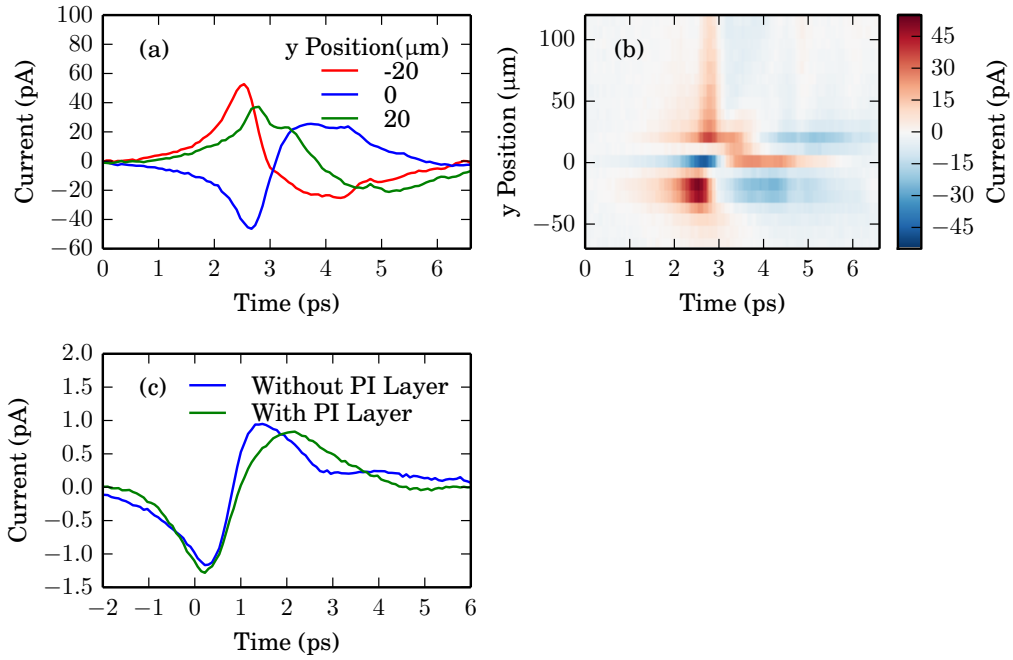

Fig. 3. (a) shows time domains scans from a SI-GaAs LPD emitter, with the optical beam positioned on the gold boundary at 0 μm and ± 20 μm from the boundary. (b) combines a set of time domain scans with lateral position demonstrating the change in polarity on the gold boundary. (c) shows the THz time domain scan of an unannealed LTG GaAs LPD emitter with and without an insulating PI layer between the metal and semiconductor.

5. Polarisation dependency

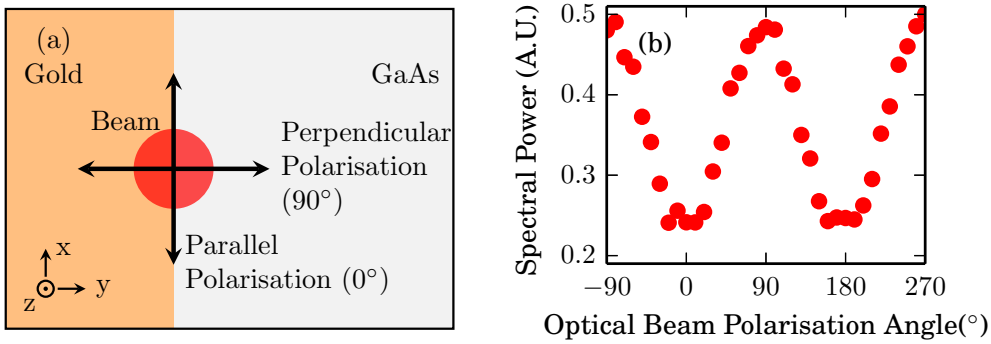

Fig. 4. (a) illustrates the polarisation orientation relative to the LPD emitter with arrows representing the polarisation of the optical beam. (b) shows the variation in THz pulse power for a SI-GaAs LPD emitter at 237 μJ cm^{-2} optical fluence. Peak THz emission occurs with perpendicularly polarised light (0°). The increased emission at perpendicular polarisation is due to the increased carrier density in the depletion region near the metal mask.

The performance of LPD emitters depends on pump polarisation relative to the gold mask.

#200985 - $15.00 USD Received 8 Nov 2013; revised 13 Dec 2013; accepted 27 Jan 2014; published 4 Feb 2014

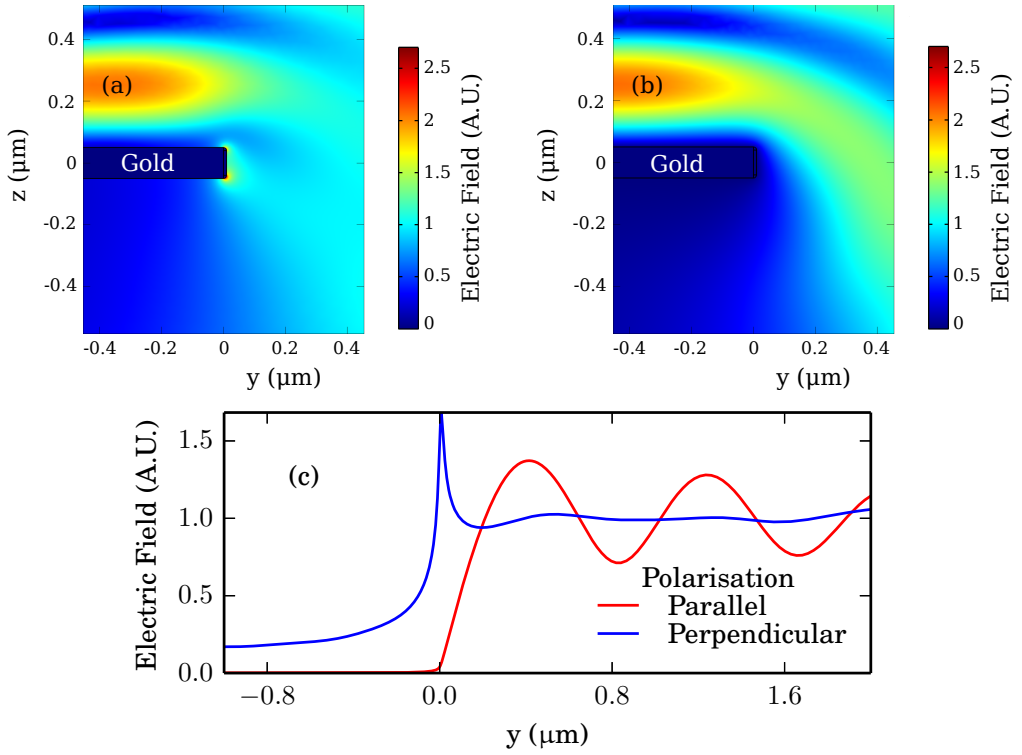

Fig. 5. (a) and (b) show the impact of polarisation on the diffracted light intensity under a 100 nm thick gold sheet in air, modelled with COMSOL. The gold masks the region $y < 0$, leaving the region $y > 0$ unmasked. The perpendicularly polarised light creates a local enhancement near the sheet edge, shown in (a). (b) shows no local enhancement for parallel polarised light. (c) shows the comparison local enhancement underneath the gold mask along the y axis.

A variation of THz output power with polarisation relative to the gold boundary was observed, as shown in Fig. 4(b). Peak output occurs with perpendicular optical polarisation. Photoconductive antennas demonstrate similar polarisation dependence, with increased output occurring with perpendicularly polarised light [21]. The increased terahertz output is attributed to an enhancement in the optical field close to the gold mask. This optical enhancement occurs within the sub-wavelength region for perpendicularly polarised light and has been calculated initially in [33]. Within photo-conductive emitters an enhancement of the electrical field exists $\sim$ 200 nm away from the anode [34, 35]. By creating an enhanced optical field near the anode more carriers are formed near the anode which experiences an enhancement in terahertz output.

We simulated the enhanced local optical field created by a LPD emitter with COMSOL. The model simulated the normalised electric field for a plane EM wave, wavelength of 800 nm, partially masked by a gold sheet, shown in Fig. 5. Figure 5(c) shows the calculated electric field at the surface of the semiconductor, showing an enhancement in the optical field within the range of 200 nm of the gold boundary for perpendicular polarisation, demonstrating the predicted local field enhancement.

LPD emission also benefits from the enhanced optical field near the gold mask. The perpendicular optical polarisation forms a higher concentration of carriers at the metal boundary. The

#200985 - $15.00 USD Received 8 Nov 2013; revised 13 Dec 2013; accepted 27 Jan 2014; published 4 Feb 2014

net diffusion current away from the metal mask is proportional to the difference between the carrier densities at the boundary and furthest from the boundary. The peak in carrier concentration caused by the local enhancement at 0 μm in Fig. 5(c) causes a higher net diffusion current away from the boundary. The increased diffusion away from the boundary creates a greater radiative dipole leading to greater LPD emission for perpendicularly polarised light.

Varying the optical polarisation also affects the fluence at which the time domain signal polarity flips. The lowest fluence required to flip the signal polarity occurs for perpendicularly polarised light. This behaviour can be explained by the increased carrier density near the metal-semiconductor interface created by the perpendicular polarisation. Due to the local optical field enhancement, more carriers are created close to the gold boundary for perpendicular polarised light. As more carriers are created within the depletion region, the current reversal as described in [20] is greater at lower fluences causing the band bending to occur at lower fluences.

6. Conclusion

We have characterised THz performance from LPD emitters for unannealed and annealed LTG GaAs and SI-GaAs. Annealed LTG GaAs has shown complex carrier dynamics owing to saturation of trap states, but further experiments are needed to understand the dynamics of the emitter where the carrier lifetime is measured as a function of fluence. Unannealed LTG GaAs demonstrated the highest saturation fluence and we conclude that for the best performance in LPD emitters annealing the sample is not required and reduces performance, resulting in a simpler fabrication process for future emitters. In the SI-GaAs sample we have shown that, as for photoconductive antennas, efficiency is increased for perpendicularly polarised light due to the increased carrier density near the gold edge. The same polarisation dependence has been observed for the annealed and unannealed LTG GaAs samples. The SI-GaAs emitter exhibits a flip in signal polarity with increasing fluence that is attributed to the Schottky contact. The Schottky THz emission from the depletion region in the metal-semiconductor boundary competes with the LPD effect. To demonstrate that the polarity flip is originating from the field of the metal-semiconductor contact we have shown that the effect can be eliminated by fabricating an emitter with an insulating layer between the metal and semiconductor.

Acknowledgments

This work was supported by the EPSRC, grants EP/G05536X/1 and EP/J007676/1. The authors would like to thank Geoff Daniell for useful discussions.

#200985 - $15.00 USD Received 8 Nov 2013; revised 13 Dec 2013; accepted 27 Jan 2014; published 4 Feb 2014